A flexible dual-mode pressure sensor with ultra-high sensitivity based on BTO@MWCNTs core-shell nanofibers

Bangze Zhou[1], Chenchen Li[1], Yanfen Zhou[1], Zhanxu Liu[1], Xue Gao[1], Xueqin Wang[1, *], Liang Jiang[1, *], Mingwei Tian[1], Fenglei Zhou[1, 2], Stephen Jerrams[3], Jianyong Yu[4]

[1] College of Textiles and Clothing, Qingdao University, Qingdao, 266071, China

[2] Centre for Medical Image Computing, University College London, London, WC1V 6LJ, UK

[3] Centre for Elastomer Research, Focas Research Institute, Technological University Dublin (TUD), City Campus, Kevin St, Dublin, D08 NF82, Ireland

[4] Innovation Center for Textile Science and Technology, Donghua University, Shanghai, 200051, China

[*] Corresponding authors, email address: liang.jiang@qdu.edu.cn; xqwang1989@163.com

Abstract

Wearable flexible sensors have developed rapidly in recent years because of their improved capacity to detect human motion in wide-ranging situations. In order to meet the requirements of flexibility and low detection limits, a new pressure sensor was fabricated based on electrospun barium titanate/multi-wall carbon nanotubes (BTO@MWCNTs) core-shell nanofibers coated with styrene-ethylene-butene-styrene block copolymer (SEBS). The sensor material (BTO@MWCNTs/SEBS) had a SEBS to BTO/MWCNTs mass ratio of 20:1 and exhibited an excellent piezoelectricity over a wide range of workable pressures from 1 to 50 kPa, higher output current of 56.37 nA and a superior piezoresistivity over a broad working range of 20 to 110 kPa in compression. The sensor also exhibited good durability and repeatability under different pressures and under long-term cyclic loading. These properties make the composite ideal for applications requiring monitoring subtle pressure changes (exhalation, pulse rate) and finger movements. The pressure sensor developed based on BTO@MWCNTs core-shell nanofibers has demonstrated great potential to be assembled into intelligent wearable devices.

Keywords: Wearable sensor, Barium titanate, Piezoelectricity, Electrospinning

1. Introduction

Recently, wearable flexible sensors have attracted much attention due to their unique mechanical properties and signal acquisition sensitivity and these properties make them excellent candidates for applications in health monitoring [1], human-machine interfacing [2], soft robotics [3], entertainment technology [4] and virtual reality [5]. Pressure sensors belong to the family of wearable sensors [6] that can be manufactured by utilizing electrical properties of materials such as piezoelectricity [7], triboelectricity [8], capacitance [9], and piezoresistivity [2, 10]. Particularly, piezoelectric pressure sensors have attracted increasing interest due to their high sensitivity and fast response times [11]. In order to realize their further applications in wearable intelligent devices, many research projects focused on developing flexible pressure sensors by incorporating piezoelectric particles into flexible elastomers, such as styrene-ethylene-butene-styrene block copolymer (SEBS) [12], thermoplastic polyurethane (TPU) [13], styrene-butadiene-styrene block copolymer (SBS) [14, 15], polydimethylsiloxane (PDMS) [16] and polyvinylidene difluoride (PVDF) [17]. These piezoelectric fillers primarily contained zinc oxide (ZnO) [18], barium titanate ($BaTiO_3$, BTO) [19] and lead titanate ($PbTiO_3$) [20].

Nontoxic BTO possessing good dielectric properties, ferroelectric properties and piezoelectric properties has been widely used in the application of nano energy generators [21]. For example, Yang et al. [17] fabricated a pressure sensor by using PVDF and polydopamine modified BTO, which exhibited a fast response time of 61 ms and a remarkable piezoelectric output voltage of 9.3 V. Hyeon et al [19] proposed a novel approach for transferring BTO thin films onto a single flexible polyimide substrate via piecemeal elimination of the sacrificial mica substrates. The sensor so fabricated converted an open-circuit voltage of 0.5 V and a short-circuit current of 30 nA from repeated bending deformations. Additionally, it has been reported that the

piezoelectric property of BTO was significantly influenced by the shape and the size of particles.

By comparison with spherical BTO particles, linear BTO particles exhibited superior piezoelectric properties [22]. Furthermore, it was found that the electrical poling process and conducting supplement filler also contributed to the further enhancement of the piezoelectric performances. This is mainly because the electric poling process can be utilized to rearrange the piezoelectric dipoles into an identical direction and results in the enhancement of electrical output performance of the electronic devices [23]. MWCNTs, which have high mechanical strength and excellent electrical properties, can be used as the conducting supplement filler to enhance the piezoelectric properties of BTO. However, due to the presence of strong van der Waals forces, MWCNTs can agglomerate easily and this has led to leakage current generation, large energy consumption and finally a reduction in electrical properties [24].

In order to solve these problems, a core-shell structured BTO@MWCNTs nanofiber was fabricated by in-situ deposition of BTO on MWCNTs via coaxial electrospinning technology. In this way, MWCNTs were evenly distributed in BTO nanofibers and thus the number of agglomerates of MWCNTs was greatly reduced. Afterwards, SEBS was coated on the BTO@MWCNTs core-shell nanofibers by doctor blading in order to fabricate a flexible pressure sensor. The results showed that the fabricated BTO@MWCNTs/SEBS pressure sensors had not only excellent piezoelectricity but also piezoresistivity and they were capable of sensing in an ultra-wide working range (1 to 50, and 20 to 110 kPa in compression) with reliable electromechanical stability, which conquered the drawback of small detection range for piezoelectric pressure sensors. Finally, the pressure sensor obtained was proposed for monitoring the physical movements of the human body. It was found that the sensing performance of BTO@MWCNTs/SEBS composites could allow the detection of not only

subtle pressures (exhalation, pulse rate), but also of large pressures (finger movement, walking), offering a promising application for implanting in smart wearable devices.

2. Experiment

2.1. Materials

SEBS G1651H (EP/PS = 67/33 wt.%) was supplied by Kraton Corporation, USA. Tetrahydrofuran (THF) and ethanol (EtOH) were purchased from Sinopharm Chemical Reagent Co., Ltd, China. Polyvinyl pyrrolidone (PVP, Mw=1300000), barium acetate ($BaAc_2$), titanium butoxide (TBT) and acetate (HAc) were supplied by Shanghai Macklin Biochemical Co., Ltd, China. MWCNTs were purchased from Shenzhen Tuling Evolution Technology Co., Ltd. Silver nanowires (AgNWs) were purchased from Beijing Deke Daojin Science and Technology Co., Ltd, China. Poly-m-phenyleneisophthalamide (PMIA) nonwoven fabric of thickness 0.3 mm was provided by Jiangsu Kaidun New Material Co., Ltd, China. Deionized water (H_2O) was made in-house.

2.2. Preparation of BTO@MWCNTs core-shell nanofibers

PVP and EtOH were mixed with PVP at concentrations of 10 wt% and 30 wt% respectively and stirred for 12 h. Next, 2.185 g $BaAc_2$, 0.815 g H_2O and 3.27 g HAc were mixed and stirred for 1 h until the solution became clear. Then 2.924 g TBT was added dropwise into the solution and stirred for 30 min. The full reaction processes are described in Equations 1 and 2. Subsequently, 0.717 g of PVP solution with a concentration of 30 wt% was mixed with the solution in a 1:4 mass ratio of PVP and BTO, and stirred for 1 h. The prepared solution was denoted as the ‘shell solution’. For the preparation of the core solution, MWCNTs were mixed with 10 wt% PVP solution at different mass ratios for each constituent (1:10, 1:8, 1:6, and 1:4) for 1 h. Then the composite was treated by ultrasonication working at 240 W and 50 kHz for 30 min.

$$Ti(OC_4H_9)_4 + 8CH_3COOH \rightleftharpoons H_4TiO_4 + 4(CH_3CO)_2O + 4C_4H_9OH \quad (1)$$

$$H_4TiO_4 + Ba(CH_3COO)_2 \longrightarrow CH_3COOH + H_2O + BaTiO_3 \quad (2)$$

BTO@MWCNTs nanofibers were prepared by using the coaxial electrospinning method. Core solution and shell solution were loaded into 10 ml syringes connected to a coaxial spinneret (core diameter of 0.71 mm, shell diameter of 1.5 mm), and fixed onto a syringe pump. The whole electrospinning process was carried out for 4 h at room temperature, humidity of 30 ~ 40%, applied voltage of 17 kV, a solution injection speed of 2 mL/h for the shell solution, and 1.5 mL/h for the core solution, drum collector rotational speed of 800 rev/min with a needle tip to collector distance of 15 cm. Then, the electrospun nanofibers were placed into a vacuum oven at 70 °C for 1 h, and the nanofibers obtained were moved to a tube furnace and annealed at 800 °C in a nitrogen atmosphere for 2 h at a ramping rate of 2 °C/min to crystallize the BTO. Finally, the BTO@MWCNTs core-shell nanofibers with 1:10, 1:8, 1:6 and 1:4 mass ratios of MWCNTs and PVP in the core solution were successfully fabricated. The whole procedure is depicted in Figures 1a and 1b.

2.2. Preparation of a flexible electrode

As shown in Figure 1c, a PMIA mat was soaked in a 0.3 wt% AgNWs ethanol solution for 5 s. Then, the mat was placed in a vacuum oven at 70 °C for 3 h. Thereafter, the above steps were repeated. Finally, the PMIA/AgNWs flexible electrodes were successfully fabricated with sheet resistances as low as 1.37 ± 0.23 Ω/sq.

2.3 Fabrication of the BTO@MWCNTs/SEBS pressure sensor

SEBS and THF were mixed with a SEBS concentration of 20 wt% for 12 h. Following this, the SEBS solution was coated on the surface of BTO@MWCNTs core-shell nanofibers with a mass ratio of SEBS to nanofibers of 4:1 by doctor blading. Afterwards, the composite was dried in a vacuum oven at 70 °C for 3 h. Finally, PMIA/AgNWs flexible electrodes were cut into the required shape and attached to the composite to obtain a flexible pressure sensor.

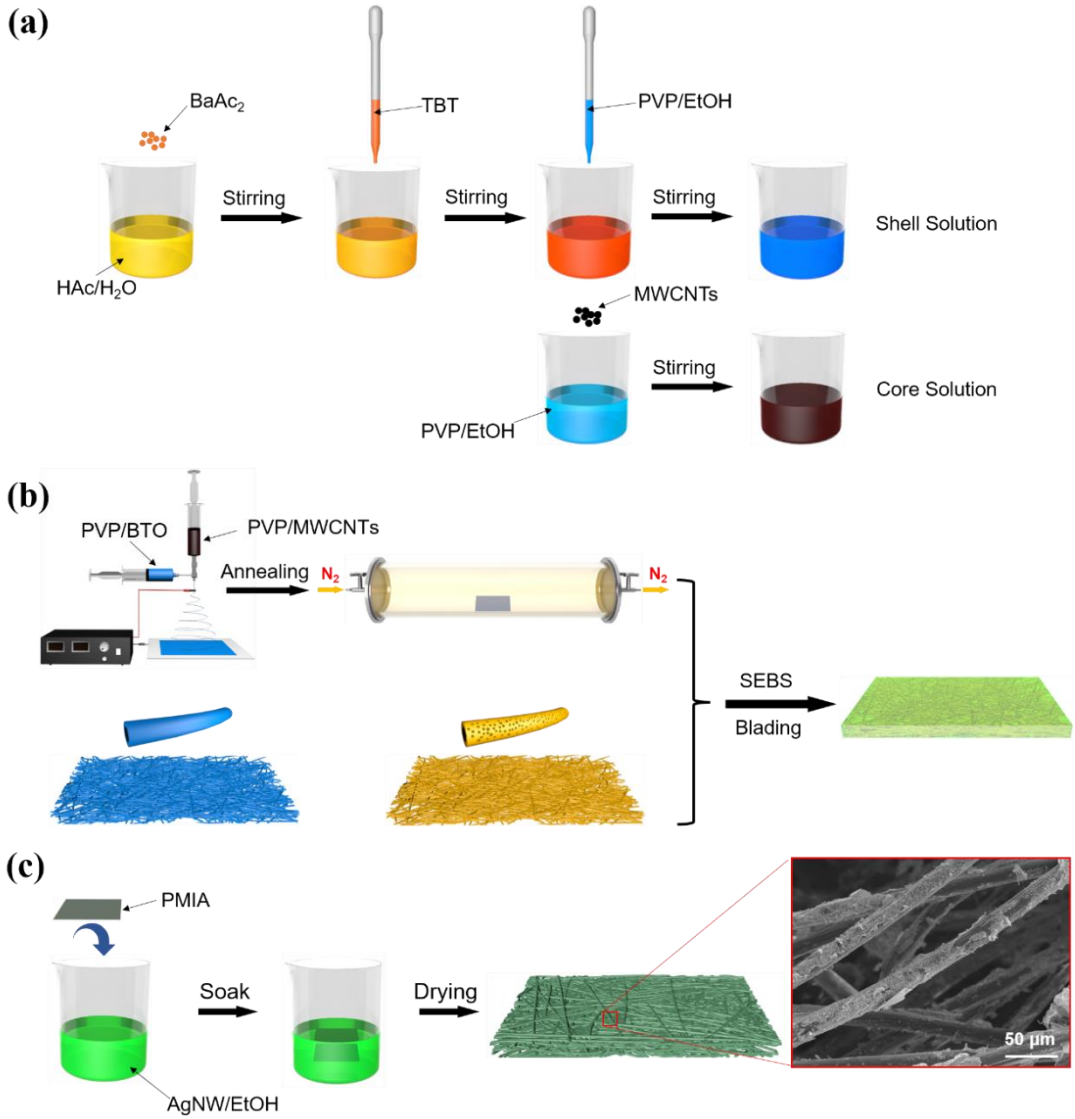

Figure 1 Illustrations of (a) preparation of core and shell solutions, (b) fabrication of BTO@MWCNTs core-shell nanofibers and (c) fabrication of PMIA/AgNW flexible electrodes.

2.4 Characterization

The morphologies of the nanofibers were investigated by scanning electron microscopy (SEM, Hitachi Regulus 8100, Japan). The SEM was equipped with an energy-dispersive X-ray analyzer (EDX). The phase structures of nanofibers were characterized by X-ray diffraction (XRD) with Cu Kα radiation on a 2 theta angle from 10° to 80°. Raman spectroscopy (DXR2, Thermo Fisher, USA) was used to characterize the molecular structure of the materials. The surface chemical composition of the fibers was determined by X-ray photoelectron

spectroscopy (XPS, Axis Supra+, Kratos, Japan) with Al Kα radiation, which was used at 15 kV and 10 mA. The C 1s peak was shifted to 284.8 eV for energy calibration. A DSC/TG synchronous thermal analyzer (STA449 F3 Jupiter, Bavaria, Germany) was used to do the thermogravimetric (TG) analysis. The test was carried out in a nitrogen atmosphere. The sample, with a weight of about 5 mg, was heated from ambient temperature to 800 ℃ at a heating rate of 10 ℃/min. A universal testing machine (Instron 5965, Glenview, USA) was used to evaluate mechanical properties under standard conditions (25 ℃/65% RH) with a uniaxial tensile force applied at a feed rate of 100 mm/min. The size of each sample was 10 mm in width, 40 mm in length and 0.3 mm in thickness. Electromechanical properties of the composite were determined by employing a digital multimeter (KEYSIGHTB2901A, Keysight Technology, USA), which was equipped with a digital push & pull tester (SHSIWI, China) and a stepper motor to apply pressure to the samples.

3. Results and discussion

SEM images of the electrospun BTO nanofibers are shown in Figure 2a and 2b. It can be seen from the figure that the BTO nanofiber had a uniform and clean surface with a single fiber diameter of 0.67 ± 0.13 μm. The EDX analysis (Figure 2c-f) showed that the nanofibers contained C, O, Ba and Ti elements, while the presence of N and Au was due respectively to residual N_2 during calcination and gold layers sprayed before SEM observation. For further confirmation of the existence of BTO, XRD was applied to investigate the crystalline structure. Figure 2g shows the XRD pattern of BTO. This depicted well-defined perovskite peaks with high intensity. The position of the peaks was consistent with XRD results reported previously [25]. The surface and cross-section morphology of BTO@MWCNTs core-shell nanofibers are presented in Figure 2h and 2i. It can be seen that BTO@MWCNTs nanofiber had an apparent core-shell structure and a single fiber diameter of 1.46 ± 0.11 μm, which meant the BTO@MWCNTs core-shell nanofibers were successfully fabricated.

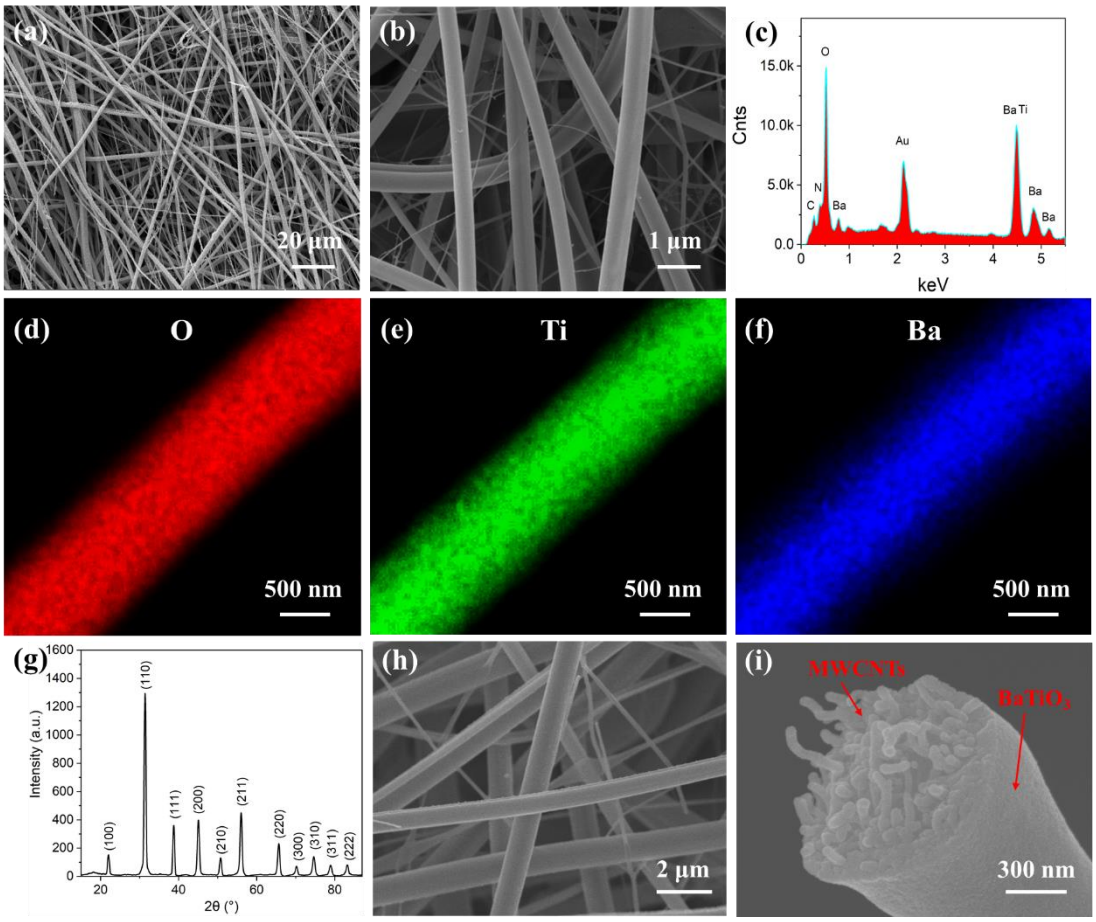

Figure 2 SEM images of BTO nanofibers at the magnification of (a) 2k and (b) 10k; (c) EDX spectroscopy of BTO nanofibers; EDX mapping images of BTO nanofibers for (d) O, (e) Ba, and (f) Ti; (g) XRD patterns of BTO nanofibers; (h) Surface and (i) cross-section morphologies of BTO@MWCNTs core-shell nanofibers.

To measure the quantity of MWCNTs in the BTO@MWCNTs core-shell nanofibers, TG analysis was carried out according to the different decomposition temperatures of BTO and MWCNTs in air. Figure 3a and 3b show the diagrams of BTO and BTO@MWCNTs core-shell nanofibers and SEM of BTO@MWCNTs core-shell nanofibers before and after calcination in air. As shown in Figure 3c, the weight loss of BTO@MWCNTs nanofibers decreased in the temperature range of 50 ℃ to 800 ℃. The content of MWCNTs in the nanofibers are summarized in Figure 3d. The amount by weight of MWCNTs were 2.47%, 3.37%, 4.76% and 7.63% when the mass ratios of MWCNTs and PVP in the core solution were 1:10, 1:8, 1:6 and

1:4, respectively. By calculation, the mass ratios of BTO and MWCNTs was 39:1, 29:1, 20:1 and 12:1, respectively. The composites with different mass ratios of BTO and MWCNTs were denoted as xBTO@yMWCNTs in the following text, where x and y represented the mass ratios of BTO and MWCNTs, respectively.

As shown in Figure 3e, BTO@MWCNTs core-shell nanofibers were too fragile to be used for flexible sensors. Thus, SEBS was coated onto the surface of BTO@MWCNTs core-shell nanofibers by doctor blading. After coating with SEBS, the BTO@MWCNTs/SEBS composite exhibited flexibility (Figure 3f). Figure 3g shows the successful encapsulation of SEBS on MWCNTs@BTO nanofibers.

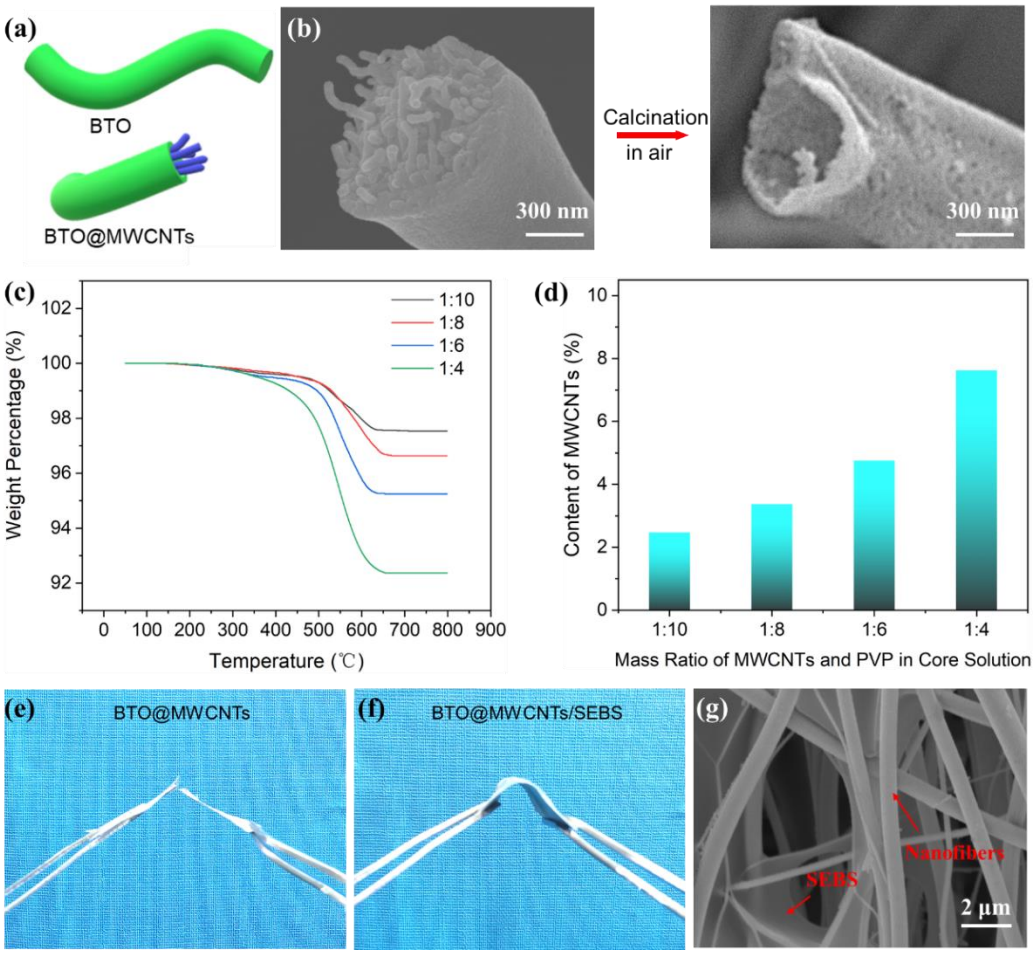

Figure 3 (a) Diagrams of BTO and BTO@MWCNTs core-shell nanofibers; (b) SEM of BTO@MWCNTs core-shell nanofibers before and after calcination in air; (c) TG curves of BTO@MWCNTs/SEBS composites with different mass ratios of BTO and MWCNTs; (d) The

relation between MWCNTs content in BTO@MWCNTs/SEBS composites and the mass ratios of BTO and MWCNTs in the core solution; (e) BTO@MWCNTs core-shell nanofibers and (f) BTO@MWCNTs/SEBS after bending; (g) SEM image of the BTO@MWCNTs/SEBS composite.

XPS spectroscopy was applied to characterize the chemical compositions of BTO, BTO@MWCNTs and BTO@MWCNTs/SEBS. As shown in Figure 4a, the peaks of C_{1s}, O_{1s}, Ti_{2p} and Ba_{3d}, which appeared in the spectra of BTO and BTO@MWCNTs, disappeared in the spectrum of BTO@MWCNTs/SEBS due to the deposition of a SEBS layer on the BTO@MWCNTs core-shell nanofibers. The appearance of O_{1s} in each spectrum was due to air pollution. Figure 4b provides the Raman spectrum of BTO, BTO@MWCNTs and BTO@MWCNTs/SEBS. It confirmed that BTO had eight Raman active modes represented by $4E(TO + LO) + 3A_1(TO + LO) + B_1(TO + LO)$. It showed the characteristic bands of the tetragonal structure at about 248 cm^{-1}, 308 cm^{-1}, 518 cm^{-1} and 720 cm^{-1} in the spectrum of BTO [26]. The peaks at around 1355 cm^{-1} and 1590 cm^{-1} in the spectrum of BTO@MWCNTs were the G band and D band respectively from MWCNTs [27]. In the spectrum of BTO@MWCNTs/SEBS, C-CH_2 stretching vibrations and C-H bending vibrations generated from SEBS appeared at 1000 and 1170 cm^{-1} respectively [28].

It is well known that good mechanical properties are essential for practical applications of engineering materials [29, 30]. As shown in Figure 4e, BTO@MWCNTs core-shell nanofibers were too fragile to undergo mechanical tensile testing. After coating with SEBS, the BTO@MWCNTs/SEBS composite could be bent and stretched. Figure 4f shows typical stress–strain curves of the BTO@MWCNTs/SEBS composite with different mass ratios of BTO and MWCNTs. The corresponding tensile strength, elongation at break and elastic modulus for each material are summarized in Figure 4g. The 39BTO@1MWCNTs/SEBS composite had a tensile strength of 0.18 MPa and an elastic modulus of 0.07 MPa. With the increase of

MWCNTs, the tensile strength and elastic modulus of BTO@MWCNTs/SEBS composite increased slightly. This was mainly due to the reinforcement of the composites by MWCNTs [31]. When the mass ratio of BTO and MWCNTs was 12:1, the tensile strength and elastic modulus were 0.19 MPa and 0.13 MPa, respectively. Meanwhile, the elongation at break of the composites decreased from 11.36% to 8.54% with the decrease of the mass ratio of BTO and MWCNTs from 39:1 to 12:1. Overall, the variation in mechanical properties among these composites was minor.

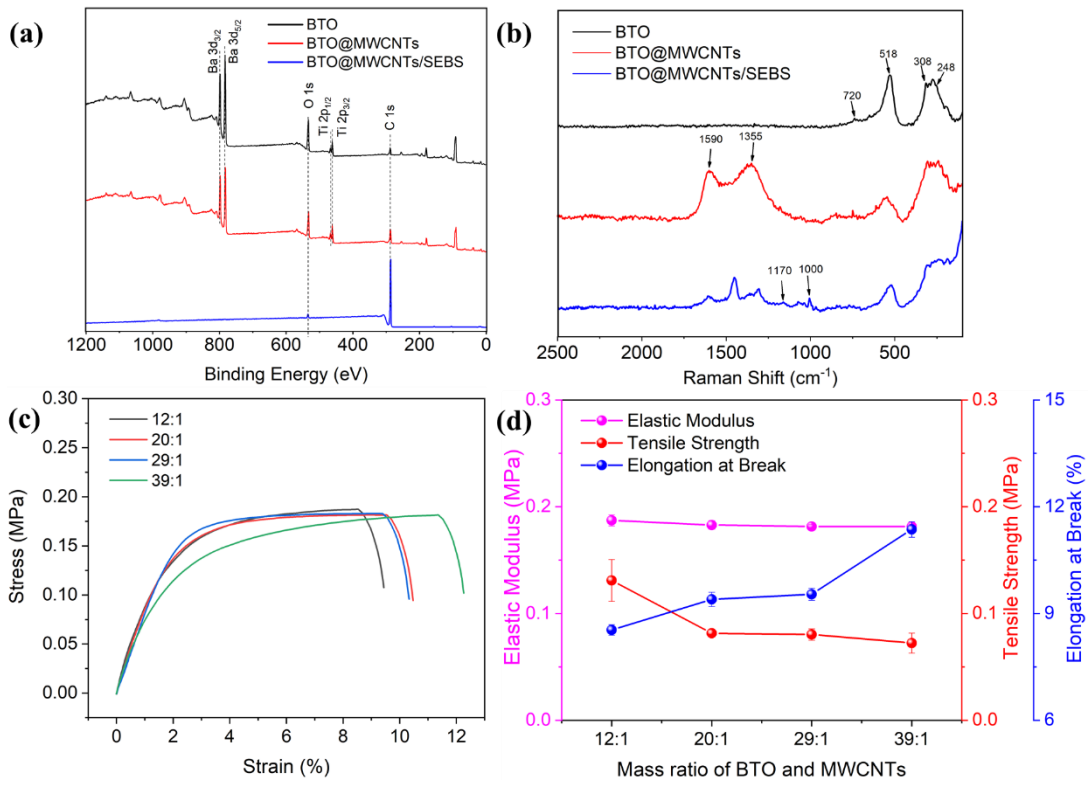

Figure 4 (a) XPS wide scan spectra of BTO, BTO@MWCNTs and BTO@MWCNTs/SEBS composite; (b) Raman spectra of BTO, BTO@MWCNTs and BTO@MWCNTs/SEBS composite; (c) Stress–strain curves of BTO@MWCNTs/SEBS composite with different mass ratios of BTO and MWCNTs; (d) Elastic modulus, tensile strength and elongation at break of BTO@MWCNTs/SEBS composite.

To investigate the piezoelectric properties of the composite, a piezoelectric sensor was fabricated by attaching a BTO@MWCNTs/SEBS composite membrane onto the shaped

PMIA/AgNW mat as an electrode and then covering this with two transparent polyethylene terephthalate (PET) membranes to prevent exposure to humid air (Figure 5a). The relationship between the mass ratios of MWCNTs in the membranes and their electromechanical properties was studied, and the results during a cyclic loading-unloading process are shown in Figure 5b-f. The schematic illustration of piezoelectric sensor under pressure can be seen from Figure 5g. When different pressures were applied to the composite membranes, the output current changed accordingly as shown in Figure 5h. Obviously, with the mass percentage of MWNCTs increased, the workable pressure range became wider, and the output current increased until the mass ratio of BTO/MWCNTs was 20:1, the highest output current reached 56.37 nA while the workable pressure range was 1 ~ 50 kPa. When the mass ratio of BTO/MWCNTs was 12:1, the output current decreased. These results can be explained well by percolation theory [32]. SEBS, BTO and MWCNTs are considered as non-conductive phase, piezoelectric phase and conductive phase, respectively. The piezoelectric property of the composite was determined by the piezoelectric effect of BTO and the increase in the amount of MWNCTs could have improved the conductive property of composite. For low mass fractions of MWCNTs, the conductivity was very close to that of the pure BTO. With the increase of MWCNTs content in the core, SEBS, BTO and MWNCTs had a significant synergistic effect, and the piezoelectric property of the composite increased rapidly. However, when the mass fraction of MWCNTs exceeded a certain percolation, the composite could be transformed into a conductor as it exhibited a rapid increase in conductivity, which led to a reduction in piezoelectric properties. Thus, the 20BTO@1MWCNTs/SEBS composite was seen to possess the appropriate properties to be chosen for use as a piezoelectric sensor.

The response time and relaxation time for the piezoelectric pressure sensor subjected to a zero to 20 kPa cyclic compression load were investigated and the results are shown in Figure 5i. It exhibited a fast response time of 20 ms and a relaxation time of 40 ms, respectively. In order

to evaluate the mechanical durability of the piezoelectric pressure sensor, a cyclic test under tensile loading was performed between a minimum load of zero and a maximum compression load of 20 kPa. As shown in Figure 5j, the change in the resistance kept stable during 7700 cycles at a frequency of 0.38 Hz. Thereafter, the piezoelectric pressure sensor exhibited good durability. Furthermore, the 20BTO@1MWCNTs/SEBS based sensor was used to detect human motion. Informed consent was obtained from the volunteer before conducting the tests. In Figure 5k-m, the sensor was shown to be capable of monitoring breath when placed 10 cm from the volunteer's nose. When the composite was attached to the volunteer's wrist and finger, current was recorded and this current varied with change in angle of finger bending. These tests significantly demonstrated the potential application of the pressure sensor for monitoring human motion.

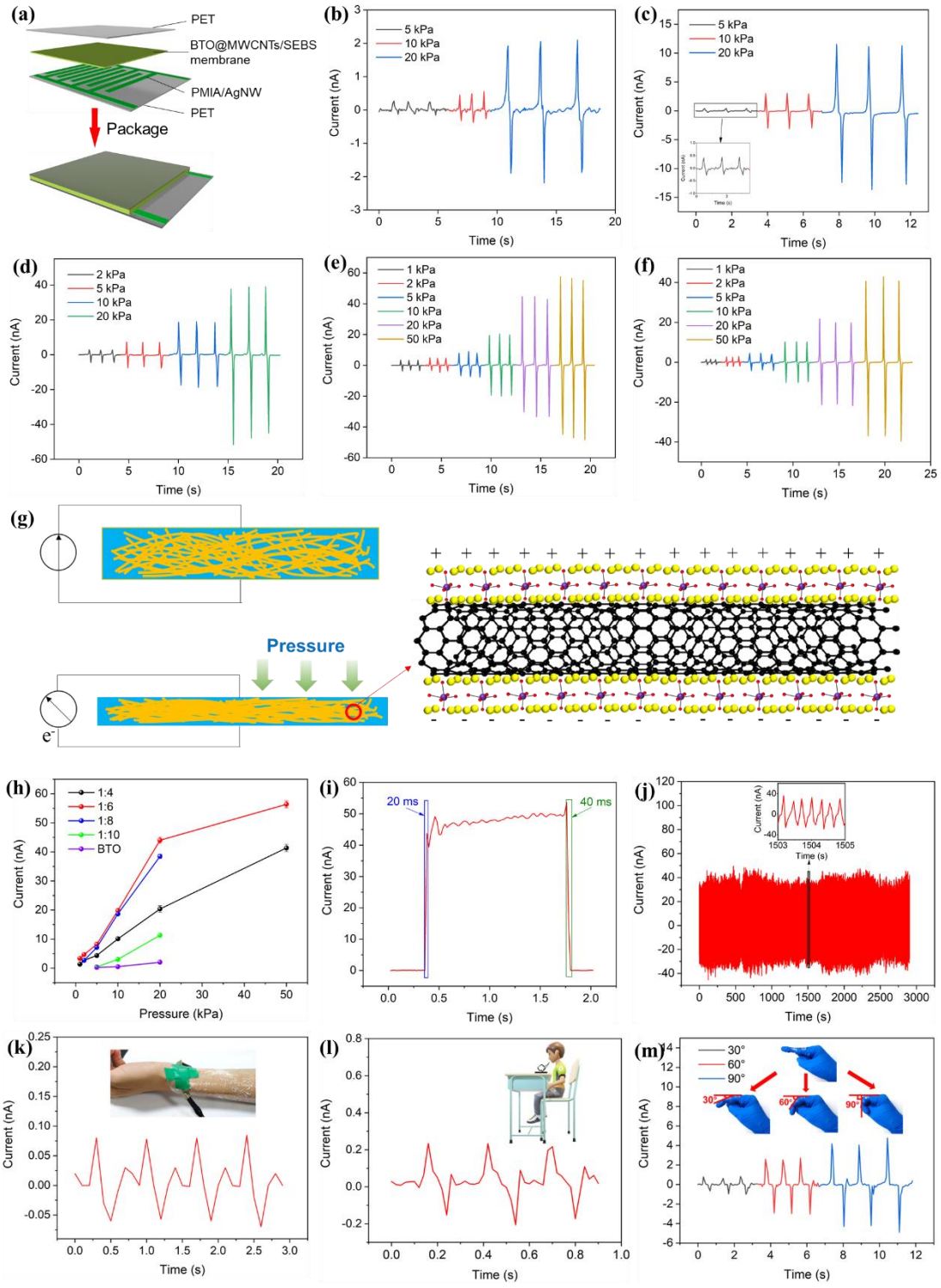

Figure 5 (a) The schematic structure of piezoelectric sensor; Current output across varied pressure of (b) pure BTO/SEBS composite, (c) 39BTO@1MWCNTs/SEBS, (d) 29BTO1MWCNTs/SEBS, (e) 20BTO@1MWCNTs/SEBS, and (f) 12BTO@1MWCNTs/SEBS; (g) The schematic illustration of longitudinal sections of

piezoelectric sensor under pressure; (h) Summary of output currents; (i) Response time of 20BTO@1MWCNTs/SEBS composite under 20 kPa; (j) 7700 cycles at the pressure of 20 kPa at a frequency of 0.38 Hz; Piezoelectric sensor used to monitor human motions, (k) pulse rate (l) exhalation, and (m) finger bending.

Also, it was found that the pressure sensor sandwiched by two PMIA/AgNWs flexible electrodes and then covered with PET membranes (Figure 6a) delivered an excellent piezoresistive performance, which greatly extended the working range of the BTO@MWCNTs/SEBS pressure sensor from 1 to 50 kPa in compression to 1 to 110 kPa in compression. Relative resistance ($\Delta R/R_0$, where ΔR represents the real-time resistance change, R is the measured resistance and R_0 represents the initial resistance) was used to characterize the change of resistance. It can be seen from Figure 6b that the resistance of sensor changed under pressure. Sensitivity of the piezoresistive sensor was defined as $S = (\Delta R/R_0)/\Delta P$, where ΔP is the relative change in applied pressure. Under pressure loads in the range 20 to 110 kPa, the sensitivity was 0.2 kPa^{-1}, which confirmed that the sensor had dual-mode and wide working range of sensor. Hysteresis (H) [33] also plays a critical role in the performance, which is defined as $H = (\pm\Delta H_{max}/Y_{FS})\times 100\%$, where ΔH_{max} stands for the maximum difference in the ordinate of the curve at the same pressure during loading and unloading, and Y_{FS} represents the maximum ordinate in the full range. By calculation, the hysteresis was 5.01% (Figure 6c).

The sensitivity and workable pressure were compared with piezoresistive sensors recently reported and summarized in Table 1. Obviously, the sensor in this work had wide workable pressure and good sensitivity. As can be observed from Figure 6d, the BTO@MWCNTs/SEBS sensor showed excellent repeatability and stability over a wide pressure range, revealing its ability to detect different external stimuli. Meanwhile, the response time and relaxation time for the piezoresistive sensor between 0 to 100 kPa compression were investigated. As shown in Figure 6e, the sensor exhibited a fast response time of 50 ms and a relaxation time of 100

ms, respectively. To evaluate the mechanical durability of the piezoresistive sensor, the loading-unloading test from 0 to 100 kPa compression was performed. As shown in Figure 6f, the change in the resistance stabilized throughout the application of 5000 cycles at a frequency of 1 Hz. Thereafter, this piezoresistive sensor exhibited good durability. It was also found that the fabricated BTO@MWCNTs/SEBS sensor could record the resistance, indicating the ability of detecting the motion of walking when attached to the insole (Figure 6g). These results demonstrated the potential application of the pressure sensor for monitoring human motion. Furthermore, by changing the counterpoises of different loading to the pressure sensor, the brightness of a bulb included in the circuit can be controlled (Figure 6h). This means that the fabricated composite can be used as a pressure rheostat.

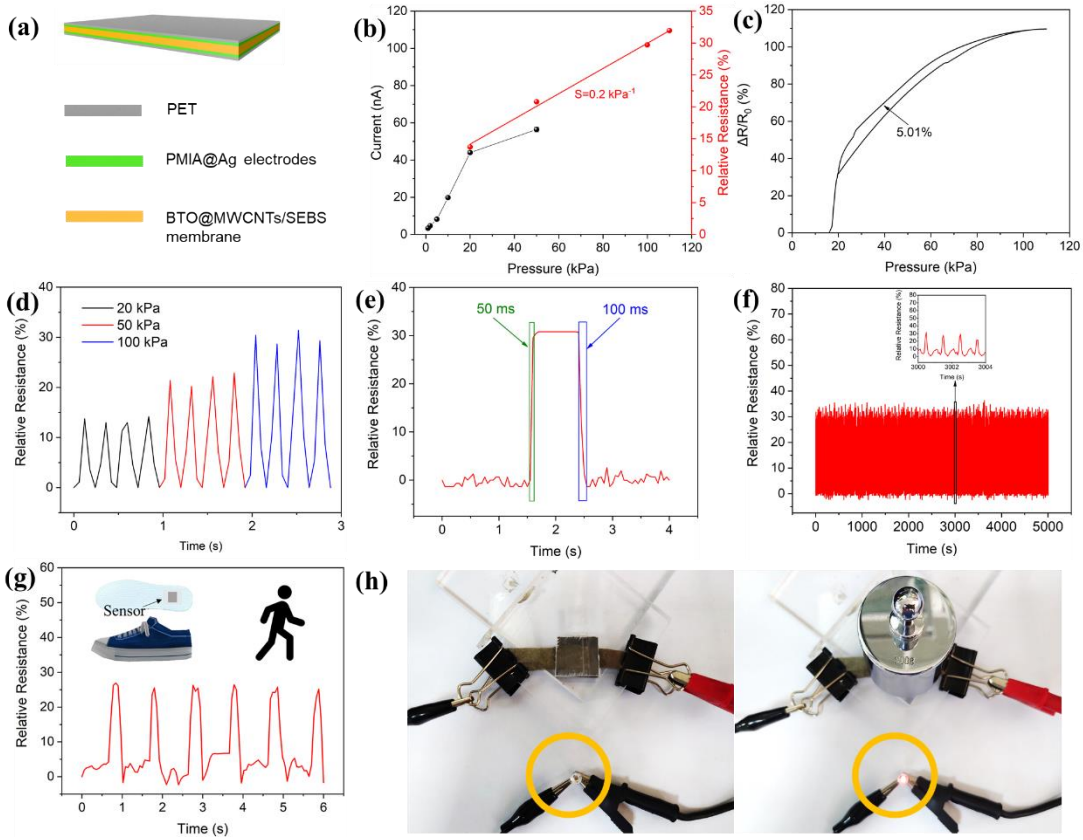

Figure 6 (a) The schematic structure of piezoresistive sensor; (b) The relative output current– and resistance–pressure curve of the 20BTO@1MWCNTs/SEBS composite; (c) The change of relative resistance of 20BTO@1MWCNTs/SEBS composite under one loading-unloading

cycle, showing hysteresis; (d) The change of relative resistance of 20BTO@1MWCNTs/SEBS composite under varied pressures of up to 100 kPa; (e) Response time of the 20BTO@1MWCNTs/SEBS composite under 100 kPa compression loading; (f) 5000 cycles in the compression pressure range 0 to 100 kPa at a frequency of 1 Hz; (g) The 20BTO@1MWCNTs/SEBS composite used to monitor walking; (h) The brightness of the bulb under different loads.

Table 1 Comparison of the piezoresistive sensors for previous and present work.

Piezoresistive Sensor	Workable Pressure (kPa)	Sensitivity (kPa^{-1})
MX/rGO Aerogel [34]	0 ~ 3.5	22.56
CuNW@G Core–Shell Aerogels [35]	0.64 ~ 35	0.00711
AgNW/TPU Membrane [36]	9.0×10^{-3} ~ 0.98	7.24
Gr/PDMS [37]	0.7 ~ 10	0.034
CNT /Tissue Paper [38]	0.035 ~ 2.5 2.5 ~ 11.7	2.2 1.3
MWCNTs/TPU [13]	0 ~ 0.2 0.2 ~ 1 1 ~ 10	2 0.5 0.02
rGo/PU [39]	0 ~ 2 2 ~ 10	0.26 0.03
This Work	20 ~ 110	0.2

4. Conclusions

In this study, a new pressure sensor possessing an ultra-wide working range with both excellent piezoelectric and piezoresistive properties was fabricated by using electrospun BTO@MWCNTs core-shell nanofibers coated with SEBS. The 20BTO@1MWCNTs/SEBS composite exhibited a piezoelectricity with a working pressure range as wide as 1 to 50 kPa in compression and an output current as high as of 56.97 nA. With reliable durability and

repeatability under different pressures and long-term cyclic loading, the 20BTO@1MWCNTs/SEBS sensor demonstrated superior performance in monitoring both subtle pressure (e.g. exhalation, pulse rate) and finger movement. Additionally, the BTO@MWCNTs/SEBS sensor exhibited a piezoresistive performance under high pressure loads (20 ~ 110 kPa), which significantly broadened its working range. With both excellent piezoelectric and piezoresistive performance, the developed BTO@MWCNTs/SEBS pressure sensor has great potential for use as a component for intelligent wearable devices.

Acknowledgements

The authors gratefully acknowledge the National Natural Science Foundation of China (Grant no. 51703108 and Grant no. 52003130), the Postdoctoral Science Foundation of China (Grant no. 2019M652318) and Taishan Scholar Foundation of Shandong, China (Grant no. tsqn201909100) for financial support.

References

[1] S. Lim, D. Son, J. Kim, Y.B. Lee, J.K. Song, S. Choi, D.J. Lee, J.H. Kim, M. Lee, T. Hyeon, D.H. Kim, Transparent and Stretchable Interactive Human Machine Interface Based on Patterned Graphene Heterostructures, Adv Funct Mater 25(3) (2015) 375-383.

[2] S. Li, R. Li, O.G. González, T. Chen, X. Xiao, Highly sensitive and flexible piezoresistive sensor based on c-MWCNTs decorated TPU electrospun fibrous network for human motion detection, Compos Sci Technol 203 (2021) 108617.

[3] C. Yan, J. Wang, W. Kang, M. Cui, X. Wang, C.Y. Foo, K.J. Chee, P.S. Lee, Highly stretchable piezoresistive graphene-nanocellulose nanopaper for strain sensors, Adv Mater 26(13) (2014) 2022-7.

[4] M. Amjadi, K.U. Kyung, I. Park, M. Sitti, Stretchable, Skin-Mountable, and Wearable Strain Sensors and Their Potential Applications: A Review, Adv Funct Mater 26(11) (2016) 1678-1698.

[5] M. Amjadi, Y.J. Yoon, I. Park, Ultra-stretchable and skin-mountable strain sensors using carbon nanotubes-Ecoflex nanocomposites, Nanotechnology 26(37) (2015) 375501.
[6] J. Heikenfeld, A. Jajack, J. Rogers, P. Gutruf, L. Tian, T. Pan, R. Li, M. Khine, J. Kim, J. Wang, J. Kim, Wearable sensors: modalities, challenges, and prospects, Lab Chip 18(2) (2018) 217-248.
[7] S.M. Villa, V.M. Mazzola, T. Santaniello, E. Locatelli, M. Maturi, L. Migliorini, I. Monaco, C. Lenardi, M. Comes Franchini, P. Milani, Soft Piezoionic/Piezoelectric Nanocomposites Based on Ionogel/BaTiO3 Nanoparticles for Low Frequency and Directional Discriminative Pressure Sensing, ACS Macro Lett 8(4) (2019) 414-420.
[8] A. Alsaadi, Y. Shi, L. Pan, J. Tao, Y. Jia, Vibration energy harvesting of multifunctional carbon fibre composite laminate structures, Compos Sci Technol 178 (2019) 1-10.
[9] S. Li, K. Dong, R. Li, X. Huang, T. Chen, X. Xiao, Capacitive pressure sensor inlaid a porous dielectric layer of superelastic polydimethylsiloxane in conductive fabrics for detection of human motions, Sensor Actuat A-Phys 312 (2020) 112106.
[10] V. Rana, P. Gangwar, J.S. Meena, A.K. Ramesh, K.N. Bhat, S. Das, P. Singh, A highly sensitive wearable flexible strain sensor based on polycrystalline MoS2 thin film, Nanotechnology 31(38) (2020) 385501.
[11] C. Wang, X. Li, E. Gao, M. Jian, K. Xia, Q. Wang, Z. Xu, T. Ren, Y. Zhang, Carbonized Silk Fabric for Ultrastretchable, Highly Sensitive, and Wearable Strain Sensors, Adv Mater 28(31) (2016) 6640-8.
[12] B.Z. Zhou, Z.X. Liu, C.C. Li, M.S. Liu, L. Jiang, Y.F. Zhou, F.L. Zhou, S.J. Chen, S. Jerrams, J.Y. Yu, A Highly Stretchable and Sensitive Strain Sensor Based on Dopamine Modified Electrospun SEBS Fibers and MWCNTs with Carboxylation, Adv Electron Mater 7(8) (2021) 2100233.

[13] J. Huang, D. Li, M. Zhao, A. Mensah, P. Lv, X. Tian, F. Huang, H. Ke, Q. Wei, Highly Sensitive and Stretchable CNT-Bridged AgNP Strain Sensor Based on TPU Electrospun Membrane for Human Motion Detection, Adv Electron Mater 5(6) (2019) 1900241.
[14] W.Y. Li, Y.F. Zhou, Y.H. Wang, Y. Li, L. Jiang, J.W. Ma, S.J. Chen, Highly Stretchable and Sensitive SBS/Graphene Composite Fiber for Strain Sensors, Macromol Mater Eng 305(3) (2020) 1900736.
[15] X. Wang, S. Meng, M. Tebyetekerwa, Y. Li, J. Pionteck, B. Sun, Z. Qin, M. Zhu, Highly sensitive and stretchable piezoresistive strain sensor based on conductive poly(styrene-butadiene-styrene)/few layer graphene composite fiber, Compos Part A-Appl S 105 (2018) 291-299.
[16] L. Wang, Y. Chen, L.W. Lin, H. Wang, X.W. Huang, H.G. Xue, J.F. Gao, Highly stretchable, anti-corrosive and wearable strain sensors based on the PDMS/CNTs decorated elastomer nanofiber composite, Chem Eng J 362 (2019) 89-98.
[17] Y. Yang, H. Pan, G. Xie, Y. Jiang, C. Chen, Y. Su, Y. Wang, H. Tai, Flexible piezoelectric pressure sensor based on polydopamine-modified BaTiO3/PVDF composite film for human motion monitoring, Sensor Actuat A-Phys 301 (2020) 111789.
[18] G. Wang, J. Liu, X. Liu, W. Feng, J. Yang, Extensional vibration characteristics and screening of polarization charges in a ZnO piezoelectric semiconductor nanofiber, J Appl Phys 124(9) (2018) 094502.
[19] D.Y. Hyeon, K.I. Park, Piezoelectric Flexible Energy Harvester Based on BaTiO3 Thin Film Enabled by Exfoliating the Mica Substrate, Energy Technol 7(10) (2019) 1900638.
[20] F. Li, S. Zhang, Z. Xu, L.Q. Chen, The Contributions of Polar Nanoregions to the Dielectric and Piezoelectric Responses in Domain-Engineered Relaxor-PbTiO3 Crystals, Adv Funct Mater 27(18) (2017) 1700310.

[21] H. Kim, F. Torres, D. Villagran, C. Stewart, Y. Lin, T.L.B. Tseng, 3D Printing of BaTiO3/PVDF Composites with Electric In Situ Poling for Pressure Sensor Applications, Macromol Mater Eng 302(11) (2017) 1700229.

[22] X. Huang, B. Sun, Y. Zhu, S. Li, P. Jiang, High-k polymer nanocomposites with 1D filler for dielectric and energy storage applications, Prog Mater Sci 100 (2019) 187-225.

[23] B. Dudem, D.H. Kim, L.K. Bharat, J.S. Yu, Highly-flexible piezoelectric nanogenerators with silver nanowires and barium titanate embedded composite films for mechanical energy harvesting, Appl Energ 230 (2018) 865-874.

[24] W. Obitayo, T. Liu, A Review: Carbon Nanotube-Based Piezoresistive Strain Sensors, J Sensors 2012 (2012) 1-15.

[25] J. Yuh, J.C. Nino, W.A. Sigmund, Synthesis of barium titanate (BaTiO3) nanofibers via electrospinning, Mater Lett 59(28) (2005) 3645-3647.

[26] M. Hedayati, E. Taheri-Nassaj, A. Yourdkhani, M. Borlaf, J. Zhang, M. Calame, T. Sebastian, S. Payandeh, F.J. Clemens, BaTiO3 nanotubes by co-axial electrospinning: Rheological and microstructural investigations, J Eur Ceram Soc 40(4) (2020) 1269-1279.

[27] J.C. Dong, L. Li, C. Zhang, P.M. Ma, W.F. Dong, Y.P. Huang, T.X. Liu, Ultra-highly stretchable and anisotropic SEBS/F127 fiber films equipped with an adaptive deformable carbon nanotube layer for dual-mode strain sensing, J Mater Chem A 9(34) (2021) 18294-18305.

[28] C.M. De León-Almazán, I.A. Estrada-Moreno, J.L. Olmedo-Martínez, J.L. Rivera-Armenta, Semiconducting elastomers based on polyaniline/clay nanocomposites and SEBS obtained by an alternative processing technique, Synthetic Met 268 (2020) 116460.

[29] M. Cai, H. He, X. Zhang, X. Yan, J. Li, F. Chen, D. Yuan, X. Ning, Efficient Synthesis of PVDF/PI Side-by-Side Bicomponent Nanofiber Membrane with Enhanced Mechanical Strength and Good Thermal Stability, Nanomaterials-Basel 9(1) (2018) 39.

[30] S. Wu, J. Liu, J. Cai, J. Zhao, B. Duan, S. Chen, Combining electrospinning with hot drawing process to fabricate high performance poly (L-lactic acid) nanofiber yarns for advanced nanostructured bio-textiles, Biofabrication 13(4) (2021) 045018.

[31] J.X. Lin, W.W. Wang, J.Q. Cheng, Z.X. Cui, J.H. Si, Q.T. Wang, W.Z. Chen, Modification of thermoplastic polyurethane nanofiber membranes by in situ polydopamine coating for tissue engineering, J Appl Polym Sci 137(41) (2020) 49252.

[32] C. Li, E.T. Thostenson, T.-W. Chou, Sensors and actuators based on carbon nanotubes and their composites: A review, Compos Sci Technol 68(6) (2008) 1227-1249.

[33] S. Chang, J. Li, Y. He, H. Liu, B. Cheng, A high-sensitivity and low-hysteresis flexible pressure sensor based on carbonized cotton fabric, Sensor Actuat A-Phys 294 (2019) 45-53.

[34] Y. Ma, Y. Yue, H. Zhang, F. Cheng, W. Zhao, J. Rao, S. Luo, J. Wang, X. Jiang, Z. Liu, N. Liu, Y. Gao, 3D Synergistical MXene/Reduced Graphene Oxide Aerogel for a Piezoresistive Sensor, ACS Nano 12(4) (2018) 3209-3216.

[35] S. Wu, M. Zou, X. Shi, Y. Yuan, W. Bai, M. Ding, A. Cao, Hydrophobic, Structure-Tunable Cu Nanowire@Graphene Core–Shell Aerogels for Piezoresistive Pressure Sensing, Adv Mater Technol-US 4(10) (2019) 1900470.

[36] J. Wang, Y. Lou, B. Wang, Q. Sun, M. Zhou, X. Li, Highly Sensitive, Breathable, and Flexible Pressure Sensor Based on Electrospun Membrane with Assistance of AgNW/TPU as Composite Dielectric Layer, Sensors-Basel 20(9) (2020) 2459.

[37] S. Chun, Y. Kim, H.S. Oh, G. Bae, W. Park, A highly sensitive pressure sensor using a double-layered graphene structure for tactile sensing, Nanoscale 7(27) (2015) 11652-9.

[38] Z. Zhan, R. Lin, V.T. Tran, J. An, Y. Wei, H. Du, T. Tran, W. Lu, Paper/Carbon Nanotube-Based Wearable Pressure Sensor for Physiological Signal Acquisition and Soft Robotic Skin, ACS Appl Mater Inter 9(43) (2017) 37921-37928.

[39] H.B. Yao, J. Ge, C.F. Wang, X. Wang, W. Hu, Z.J. Zheng, Y. Ni, S.H. Yu, A flexible and highly pressure-sensitive graphene-polyurethane sponge based on fractured microstructure design, Adv Mater 25(46) (2013) 6692-8.